REMARKS ON THE CALCULATION OF TRANSONIC POTENTIAL FLOW BY A FINITE VOLUME METHOD*

A. Jameson

Courant Institute of Mathematical Sciences,
New York University

1 Introduction

The purpose of this paper is to review the development of a finite volume method for the numerical calculation of transonic flow, under the assumption that the flow is irrotational, so that the velocity can be represented as the gradient of the potential. Essentially this limits the application of the method to flows containing fairly week shock waves, for which the Mach number of the normal component of the velocity ahead of the shock is not substantially greater than 1.3, since shock waves are to be modelled by isentropic jumps. This is in contrast to solutions of the Euler equation, as discussed in other papers in the present volume, for which there is an increase in entropy in traversing the shock and consequently the flow downstream of the shock is rotational. The potential flow approximation has been widely used in calculations of flows over aerofoils and wings [1,2], and found to give excellent results up to the onset of drag rise, provided that the geometric profile is corrected to allow for the displacement effect of the boundary layer.

A well-established procedure is to transform the potential flow equation into a curvilinear coordinate system which conforms to the body. This has been shown to give accurate predictions of flows past wings [1,2], cascades [3] and nacelles [4]. It becomes progressively more difficult, however, to find a suitable transformation as the geometric configuration becomes more complex, and a more flexible method will be required if the calculation are to be extended from isolated components to more complete configurations such as wing-body-tail combinations and ultimately a complete aircraft.

The present method borrows from finite-element techniques to arrive at a discretization procedure with the flexibility needed to treat arbitrary geometric configurations. This leads initially to formulas which are a central-difference approximation to the potential flow equation in conservation form. As they stand, these formulas are unsuitable for the treatment of transonic flow, because they preserve symmetry in the upwind and downwind directions. This leads to a difficulty connected with the non-uniqueness of

*Work supported by the Office of Naval Research under contract No. N00014-77-C-0032

solutions of the potential equation for transonic flow, in the absence of a condition that expansion shocks are to be excluded. If the Euler equation were being solved, instead of the potential equation, the existence of an expansion shock would imply a decrease in entropy through the shock; it would therefore be justifiable to exclude this from the numerical solution on the basis of the physical argument that entropy cannot decrease in a real flow. If the numerical solution of the potential equation is to give a reasonable representation of a real flow, steps must be taken to ensure that expansion shocks are likewise excluded. Consider for example, the flow past a body with fore and aft symmetry, such as an ellipse. The proper solution consists of a smooth expansion over the front half of the profile, followed by a discontinuous compression through a shock wave standing over the rear half. Presuming that a suitable iterative scheme could be found to solve the central-difference equations, fore and aft symmetry would be preserved in the solution, which would therefore contain an expansion shock at the front and a compression shock at the rear. In the present method this difficulty is overcome by the device of modifying the difference formulas so that they have an upwind bias in zones of supersonic flow. this procedure, first used by Murman and Cole for the numerical solution of the transonic small disturbance equation [5], has been found to lead to stable numerical schemes with effective shock-capturing properties. Whereas Murman and Cole used a simple switch to upwind differencing at supersonic points, the upwind bias is introduced here by the addition of artificial viscosity [6]. the viscosity is eliminated in zones of subsonic flow by a switching function. This leads to sharp representation of shock waves. At the same time the conservation form is preserved in the construction of the viscosity, so that according to a theorem of Lax and Wendroff [7], the proper shock-jump relation consistent with the isentropic model is yielded in the limit as the mesh width is reduced to zero. The complete difference equations with artificial viscosity added are solved by embedding the steady-state equation in an artificial time-dependent equation constructed so that it evolves to the steady-state solution [8].

An alternative approach to the problem of eliminating expansion shocks is to use an iterative scheme derived from optimal control theory, and to introduce a penalty function to limit the magnitude of the expansion gradients to be permitted in the solution. In this approach, which has been explored by Glowinski, Perrier and Pironneau [9] (see also the paper by Bristeau et al in the present volume) the desymmetrization of the solution for a body with fore and aft symmetry is accomplished by the iterative scheme rather than by direct desymmetrization of the difference formulas.

2 Formulation of the equations

As a typical application, consider the case of a wing or a wing-body combination in a uniform stream. Assuming the flow to be isentropic and to satisfy the equations of potential flow, let Φ be the potential. Also let $\underline{q}$ be the velocity vector, given by $\underline{q} = \nabla\Phi$, where ∇ is the gradient operator in cartesian space; $\underline{q}$ has the magnitude q and cartesian components *u, v, w*. Let p and ρ be pressure and density. The potential

flow equation can be written in conservation form as

$$\nabla \cdot (\rho \underline{q}) = 0$$

or, using cartesian coordinates x,y,z, as

$$\frac{\partial}{\partial x}(\rho u) + \frac{\partial}{\partial y}(\rho v) + \frac{\partial}{\partial z}(\rho w) = 0 \tag{1}$$

where

$$u = \Phi_x, \quad v = \Phi_y, \quad w = \Phi_z. \tag{2}$$

Also let a be the local speed of sound and M be the local Mach number q/a, and let M_∞, $q_\infty = 1$ and $\rho_\infty = 1$ be the Mach number, speed and density of the uniform flow at infinity. Then the local density ρ is given by the formula

$$\rho = \{1 + \frac{\gamma - 1}{2} M_\infty^2 (1 - q^2)\}^{\frac{1}{\gamma - 1}} \tag{3}$$

where γ is the ratio of specific heats, and the pressure and speed of sound follow from relations

$$p = \frac{\rho^\gamma}{\gamma M_\infty^2}, \quad a^2 = \frac{dp}{d\rho} = \frac{\rho^{\gamma - 1}}{M_\infty^2}. \tag{4}$$

Equation (1) is hyperbolic when the flow is locally supersonic, and elliptic when it is locally subsonic; furthermore, consistent with the theorem of Morawetz [10], shock waves will generally appear if there is a region of supersonic flow. The shock jump conditions which will be applied are:

(a) continuity of Φ, implying a continuity of the tangential velocity component;

(b) continuity of ρq_n, where q_n is the velocity component normal to the shock surface;

(c) the condition that q_n decrease through the shock.

According to these conditions a normal shock is to be modeled as a jump between equal-area points of an isentropic stream tube. With such a model it is not possible simultaneously to satisfy the condition that the pressure-plus-normal-momentum be conserved across the shock (in contrast to a solution of the Euler equations using the Ranking-Hugoniot relations across the shock, in which this quantity is explicitly conserved and consequently the entropy increases across the shock). Now in a non-lifting potential flow, the streamwise component of this pressure-plus-normal-momentum discontinuity integrated over the shock surface must exactly cancel that of the pressure integral over the body surface. It thus follows that this latter quantity, which may be interpreted as the drag force corresponding to a non-lifting isentropic flow, is in fact a measure of the violation of the continuity of pressure-plus-normal-momentum across the shock; it is sometimes taken as an approximation to the "wave drag" for a real flow, which is in fact related to the entropy production at the shock surface. A similar argument applies for lifting potential flow: the pressure integral over the body surface in a

potential flow solution yields a drag which simulates the wave and vortex drag.

The boundary condition at the body is that the normal velocity component be zero, that is:

$$q_n = \frac{\partial \Phi}{\partial n} = 0 \tag{5}$$

To obtain a unique lifting solution the Kutta condition that there be no flow around the trailing edge is also imposed. The resulting spanwise variation in the calculation $\Gamma = \int q \, ds$ around each wing section causes a vortex sheet to be shed from the trailing edge. In the calculations, the vortex sheet will be assumed to coincide with a coordinate surface and convection and roll-up of the sheet will be ignored. The conditions to be applied at the sheet are then

(a) the jump Γ in the potential is constant along lines parallel to the free stream

(b) the normal velocity component q_n is continuous through the sheet.

In the far field, Φ approaches the potential of the undisturbed free stream, except in the Trefftz plane far downstream, where there is a flow induced by the vortex sheet and Φ approaches a two-dimensional solution of Laplace's equation with a jump across the vortex sheet.

In a finite domain R with boundary S, equations $(1) - (5)$ are equivalent to the Bateman variational principle [11] which states that

$$I = \int_R p \, dR \tag{6}$$

is stationary. Now a variation $\delta\Phi$ in the potential produces a velocity variation given by $\delta \underline{q} = \nabla \delta\Phi$. Since inserting equation (3) into the first of equations (4) gives the pressure p as a function of the single variable q, it can easily be shown that the pressure variation p compatible with the potential variation $\delta\Phi$ is given by:

$$\delta p = -\rho \underline{q} \cdot \delta \underline{q}$$

Thus

$$\delta I = -\int_R \rho \underline{q} \cdot \nabla \, \delta\Phi \, dR$$

$$= \int_R \delta\Phi \, \nabla \cdot (\rho \underline{q}) \, dR \; - \; \int_S \delta\Phi \, \rho q_n \, dS$$

The contribution from the boundary integral vanishes when the boundary value of Φ is specified (as at the far-field boundary) or when q_n (as at the body); for δI to vanish for arbitrary $\delta\Phi$ it is necessary that equation (1) should hold throughout R.

Consider a transformation to a new set of coordinates X, Y, Z. Suppose that the derivatives of the transformation are given by

$$H = \begin{bmatrix} X_X & X_Y & X_Z \\ Y_X & Y_Y & Y_Z \\ Z_X & Z_Y & Z_Z \end{bmatrix} \quad H^{-1} = \begin{bmatrix} X_X & X_Y & X_Z \\ Y_X & Y_Y & Y_Z \\ Z_X & Z_Y & Z_Z \end{bmatrix} \tag{7}$$

and let h be the determinant of H; the value of h at a particular point is equal to the local value of the ratio of an elemental volume in the physical (distorted) cell to the corresponding elemental volume in the mapped (cubic) cell. The metric tensor of the new coordinate system is defined by the symmetric matrix

$$G = H^T H \tag{8}$$

It follows by chain rule that

$$\begin{bmatrix} u \\ v \\ w \end{bmatrix} = H^{-T} \begin{bmatrix} \Phi_X \\ \Phi_Y \\ \Phi_Z \end{bmatrix} \tag{9}$$

Also equation (1) becomes

$$\left(X_X \frac{\partial}{\partial X} + Y_X \frac{\partial}{\partial Y} + Z_X \frac{\partial}{\partial Z}\right)(\rho u) + \left(X_Y \frac{\partial}{\partial X} + Y_Y \frac{\partial}{\partial Y} + Z_Y \frac{\partial}{\partial Z}\right)(\rho v)$$
$$+ \left(X_Z \frac{\partial}{\partial X} + Y_Z \frac{\partial}{\partial Y} + Z_Z \frac{\partial}{\partial Z}\right)(\rho w) = 0$$

Then on multiplying by h and substituting the appropriate co-factors of H for quantities such as hX_X, it may be verified that equation (1) reduces to

$$\frac{\partial}{\partial X}(\rho h U) + \frac{\partial}{\partial Y}(\rho h V) + \frac{\partial}{\partial Z}(\rho h W) = 0 \tag{10}$$

where $U, V and W$ are the contravariant velocity components defined by

$$\begin{bmatrix} u \\ v \\ w \end{bmatrix} = H^{-1} \begin{bmatrix} u \\ v \\ w \end{bmatrix} = G^{-1} \begin{bmatrix} \Phi_X \\ \Phi_Y \\ \Phi_Z \end{bmatrix} \tag{11}$$

The expression on the left-hand side of equation (1) is a well-known formula of tensor analysis for the quantity $h\nabla \cdot (p\underline{q})$ [12]. It may also be verified that the speed q, appearing in equation (3) for and indirectly in equations (4) for p and a^2, is now determined by the formula:

$$q^2 = U\Phi_X + V\Phi_Y + W\Phi_Z \tag{12}$$

3 Construction of the numerical scheme

The discrete approximation to the equations will be developed using a subdivision of the domain into distorted cubic cells. It is convenient to regard each cell as being generated by a separate trilinear transformation between local coordinates X, Y, Z and cartesian coordinates x, y, z. Numbering the cell vertices from 1 to 8, as illustrated in Fig.1, the vertices in the local coordinates are assumed to be at $X_i = \pm\frac{1}{2}, Y_i =$

$\pm\frac{1}{2}, Z = \pm\frac{1}{2}$. (Note that the computational cell thus has unit volume). then the local mapping is defined by

$$x = 8 \sum_{i=1}^{8} x_i \, (\frac{1}{4} + X_i X) \, (\frac{1}{4} + Y_i Y) \, (\frac{1}{4} + Z_i Z) \tag{13}$$

with similar formulas for y, z. The potential is assumed to have a similar form inside the cell

$$\Phi = \sum_{i=1}^{8} \Phi_i \, (\frac{1}{4} + X_i X) \, (\frac{1}{4} + Y_i Y) \, (\frac{1}{4} + Z_i Z) \tag{14}$$

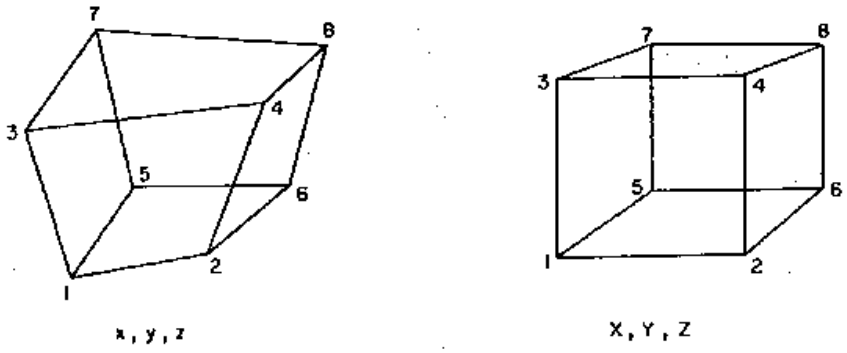

Fig. 1

This amounts to representing the solution with isoparametric trilinear finite elements [13]. Such elements preserve the continuity of x, y, z and Φ at the cell boundaries because the mappings in adjacent cells reduce to the same bilinear form at the common face.

The derivatives of the transformation, obtained by differentiating (13), in general vary throughout the volume of each cell; the determinant h is likewise variable. the derivatives at a cell centre $X = 0, \; Y = 0, \; Z = 0$, are given by formulas such as:

$$x_X = \frac{1}{4} \, (x_2 - x_1 + x_4 - x_3 + x_6 - x_5 + x_8 - x_7)$$

Let the cell vertices be represented by triple subscripts i, j, k and let quantities evaluated at the cell centres be denoted by subscripts $i + \frac{1}{2}, j + \frac{1}{2}, k + \frac{1}{2}$. It is convenient to introduce averaging and difference operators by the notation

$$\mu_X f_{i,j,k} = \frac{1}{2}(f_{i+\frac{1}{2},j,k} + f_{i-\frac{1}{2},j,k})$$

$$\delta_X f_{i,j,k} = \frac{1}{2}(f_{i+\frac{1}{2},j,k} - f_{i-\frac{1}{2},j,k})$$

Suppressing the indices, it is also convenient to use notation such as

$$\mu_{XX} f = \mu_X(\mu_X f), \quad \mu_{XY} f = \mu_X(\mu_Y f)$$
$$\delta_{XX} f = \delta_X(\delta_X f), \quad \delta_{XY} f = \delta_X(\delta_Y f)$$

By inspecting the arrangement of terms in the expression given earlier for x_X, for example, it can then be seen that the derivatives of the transformation at the cell centres are given by formulas such as

$$x_X = \mu_{YZ}\, \delta_X\, x, \qquad x_Y = \mu_{XZ}\, \delta_Y\, x;$$

similarly it follows from equation (14) that

$$\Phi_X = \mu_{YZ}\, \delta_X\, \Phi, \qquad \Phi_{XY} = \mu_Z\, \delta_{XY}\, \Phi, \qquad \Phi_{XYZ} = \delta_{XYZ}\, \Phi$$

A discrete approximation to equation (1) can now be derived by using a simple one-point integration scheme to approximate the Bateman integral given by the equation (6). Thus this integral is replaced by a sum of terms, each comprising the product of the pressure at a cell centre and the volume of that cell. Since the volume of a (distorted) cell is approximately equal to the value of the determinant at the centre of that cell, the integral is approximated by:

$$I = \sum_{i,j,k} h_{i+\frac{1}{2},j+\frac{1}{2},k+\frac{1}{2}}\; P_{i+\frac{1}{2},j+\frac{1}{2},k+\frac{1}{2}}.$$

According to equations $(3), (4)$ and (12), using (11) and the fact that G^{-1} is symmetric, the variation in p due to a variation $\delta\Phi$ may be written in the form:

$$\delta p = -\rho\delta\left(\frac{q^2}{2}\right) = -\rho\left(U\;\delta\Phi_X + V\;\delta\Phi_Y + W\;\delta\Phi_Z\right)$$

Furthermore, the solution to the problem is obtained when the value of Φ at every node is such that I is stationary, i.e. the derivative of I with respect to every nodal value $\Phi_{i,j,k}$ is zero. It then follows on setting

$$\frac{\partial I}{\partial \Phi_{i,j,k}} = 0$$

with respect to each node i, j, k, and collecting the contributions from the eight cells with this node as common vertex, that

$$\mu_{YZ}\;\delta_X\;(\rho h U) + \mu_{ZX}\;\delta_Y\;(\rho h V) + \mu_{XY}\;\delta_Z\;(\rho h W) = 0. \tag{15}$$

Along the boundary there are only four cells adjacent to each mesh point and equation (15) is correspondingly modified.

If the cell vertices are assumed to be generated by a smooth global transformation of coordinates, equation (15) can be directly interpreted as a difference approximation

to equation (10). First the derivatives of the transformation and the potential are evaluated at each cell centre by the "box scheme", in which each derivative is approximated by the average of the differences along the four cell edges in the appropriate direction. Then equation (10) is approximated by a second application of the box scheme to represent a flux balance over a set of auxiliary cells, each generated from a cube joining the centres of 8 primary cells, as illustrated in Fig.2.

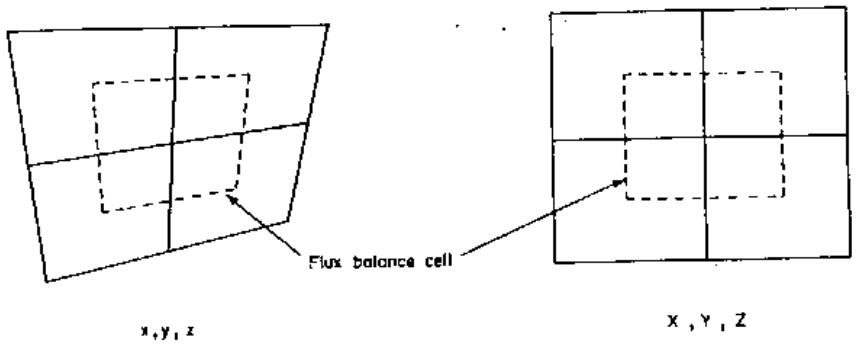

Fig. 2

With this interpretation the local discretization error is seen to be of second order as long as the transformation is smooth. The quantity ρhU represents the flux across a face X = constant and the boundary condition (5) simply reduces to $U = 0, V = 0$ or $W = 0$ on cell faces coincident with the boundary. The flux balance is then represented with auxiliary cells bounded on one or more faces by the body surface, as illustrated in Fig.3.

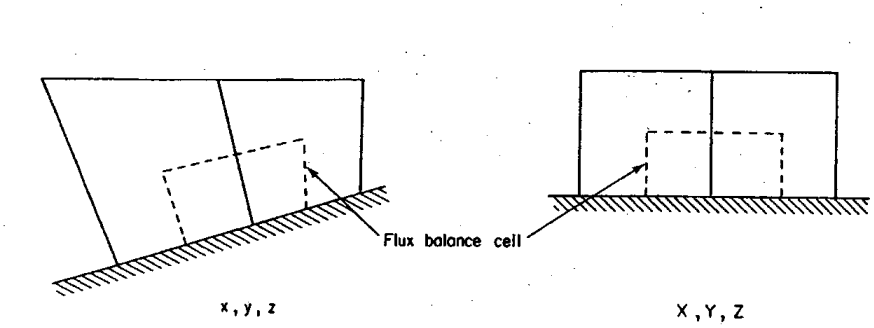

Fig. 3

The use of a more accurate integration scheme than the simple one-point formula to represent the Bateman integral would lead to a much more complicated difference

equation than equation (15). For two-dimensional calculations, equation (15) has the property that it admits the uniform flow defined by $\Phi = x$ as an exact solution, but for three-dimensional calculations it generally does not. The scheme as it stands also has a disadvantage which can most readily be seen by considering Laplace's equation on a uniform grid. Setting $h = 1, \rho = 1$, equation (15) reduces in the two-dimensional case to

$$(\mu_{YY}\delta_{XX} + \mu_{XX}\delta_{YY})\,\Phi = 0$$

which is the rotated Laplacian scheme

$$\Phi_{i+1,j+1} + \Phi_{i-1,j+1} + \Phi_{i+1,j-1} + \Phi_{i-1,j-1} - 4\Phi_{i,j} = 0$$

It can thus be seen that the discrete equation for any point i, j does not contain contributions from adjacent points in the same row or column of the mesh. It follows that the odd and even mesh points are decoupled into two independent meshes with a larger mesh interval. The solution at each point is independent of the solution at all the nodes of the other mesh (apart from any coupling effects which may be introduced at the boundary). Furthermore, it can be seen that separate uniform distributions of potential on each of these two meshes will satisfy the above rotated Laplacian scheme at all internal points of each mesh. Thus high-frequency oscillations in which, for example, $\Phi = 1$ at odd points and -1 at even points are admitted by the scheme. This difficulty can be traced to the representation of the flux across the face AB in Fig.4 by the derivative Φ_X evaluated

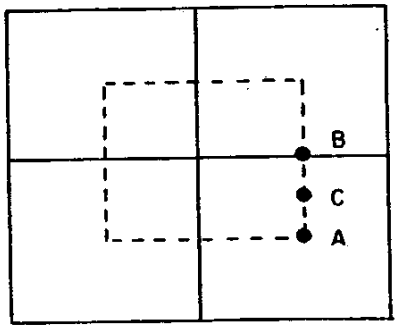

Flux at C
$= (\phi_X)_A + \epsilon\,\phi_{XY}$

Fig. 4

at the point A. This flux would be better represented by evaluating Φ_X at a point C somewhere on the face. This shift can be accomplished by adding a compensating term $\varepsilon\Phi_{XY}$ to Φ_X. The addition of similar terms on all faces produces the formula

$$(\mu_{YY}\delta_{XX} + \mu_{XX}\delta_{YY} - \varepsilon\,\delta_{XYXY})\,\Phi = 0$$

which reduces to the usual 5-point second-order-accurate formula when $\varepsilon = \frac{1}{2}$, and to the 9-point fourth-order-accurate formula when $\varepsilon = \frac{1}{3}$.

Equation (15) can be compensated in a similar manner. Allowing for the dependence of ρ on $\Phi_X,\ \Phi_Y,\ \Phi_Z$, the coefficients of $\Phi_{XX},\ \Phi_{YY},\ \Phi_{ZZ}$ when equation (10) is expanded are

$$A_X = \rho h \left(g^{11} - \frac{U^2}{a^2} \right)$$

$$A_Y = \rho h \left(g^{22} - \frac{V^2}{a^2} \right)$$

$$A_Z = \rho h \left(g^{33} - \frac{W^2}{a^2} \right)$$

where g^{ij} are the elements of G^{-1} (the algebraic manipulations used in deriving these expressions take account of the fact that G^{-1} is symmetric). These coefficients can conveniently be used to determine the magnitude of the corrections to be applied to the fluxes across the different faces of each auxiliary cell, for example, $\varepsilon A_X\ \mu_Z\ \delta_{XY}\ \Phi$ to shift Φ_X in the Y direction on a face X = constant. Let

$$Q_{XY} = (A_X + A_Y)\ \mu_Z\ \delta_{XY}\ \Phi.$$

with similar formulas for Q_{YZ}, Q_{ZX}, and let

$$Q_{XYZ} = (A_X + A_Y + A_Z)\ \delta_{XYZ}\ \Phi$$

Then collecting the contributions from the eight primary cells surrounding each mesh point, the final compensated equation is

$$\mu_{YZ}\ \delta_X\ (\rho h U) + \mu_{ZX}\ \delta_Y\ (\rho h V) + \mu_{XY}\ \delta_Z\ (\rho h W)$$

$$-\varepsilon \left\{ \mu_Z\ \delta_{XY}\ Q_{XY} + \mu_X\ \delta_{YZ}\ Q_{YZ} + \mu_Y\ \delta_{ZX}\ Q_{ZX} - \frac{1}{2}\delta_{XYZ}\ Q_{XYZ} \right\} = 0 \quad (16)$$

where $0 \leq \varepsilon \leq \frac{1}{2}$. In practice the value $\varepsilon = \frac{1}{2}$ has proved satisfactory. Observe that equation (16) is assembled by calculating all possible mixed differences as well as the first differences in the application of the box scheme to the primary cells, and then repeating the same mixed differencing operations in the second application of the box scheme to represent the flux balance.

Equation (16) completes the definition of the scheme for subsonic flow. It remains to add artificial viscosity to produce a scheme which is desymmetrized in the streamwise direction in zones of supersonic flow and will not admit expansion shocks. Equation (10) will be replaced by the modified conservation law

$$\frac{\partial}{\partial X}(\rho h U + P)\ + \frac{\partial}{\partial Y}(\rho h V + Q)\ + \frac{\partial}{\partial Z}(\rho h W + R) = 0$$

where the added fluxes P, Q and R are proportional to the cell width in the physical domain, with the result that the correct conservation law is recovered in the limit as the cell width is reduced to zero. Presuming the distribution of mesh points to be smooth,

P, Q and R are constructed as approximations to $-\mu h\,|U|\,\Delta X\ \rho_X, -\mu h\,|V|\,\Delta Y\ \rho_Y$ and $-\mu h\,|W|\,\Delta Z\ \rho_Z$, where μ is a switching function

$$\mu = \max\left[0, \left(1 - \frac{a^2}{q^2}\right)\right]$$

which vanishes in the subsonic zone, and $\Delta X, \Delta Y$ and ΔZ are the cell widths in the computational domain (each equal to unit); note that each of these terms is approximately proportional to the mean cell-width in each direction in the physical domain, since h is approximately equal to the volume of the physical cell, i.e. to the product of the mean cell-widths.

The simplest implementation is to represent $\Delta X\ \rho_X$ directly by differencing between adjacent cells. Then the effect of P, Q, and R is to replace the densities appearing in equation (15) by modified densities such as $\rho - \mu\ \delta_X\ \rho$ in the first term. In three-dimensional calculations for a swept wing, however, the cells typically have a very high aspect ratio in the spanwise direction, and this has proved unsatisfactory because the use of shifted densities at the centres of the primary cells surrounding a given mesh point does not sufficiently concentrate the artificial viscosity at that point. The following scheme has proved stable. According to formula (3)

$$\rho_X = -\frac{\rho}{a^2}\ \frac{\partial}{\partial X}\left(\frac{q^2}{2}\right)$$

where q^2 is given by the formula (12). Therefore first construct

$$\hat{p} = \mu h \frac{\rho}{a^2}\left(U^2\ \delta_{XX} + UV\ \mu_{XY}\ \delta_{XY} + WU\ \mu_{ZX}\ \delta_{ZX}\right)\Phi$$

and $\hat{Q}, \hat{R}$ by similar formulas. Then set

$$P_{i+\frac{1}{2},j,k} = \begin{cases} \hat{P}_{i,j,k} & \text{if } U > 0 \\ \hat{P}_{i+1,j,k} & \text{if } U < 0 \end{cases}$$

with similar shifts for Q, R. Finally equation (15) is modified by the addition of

$$\delta_X P + \delta_Y Q + \delta_Z R.$$

This introduces the desired upwind bias in the difference scheme at each supersonic point.

An iterative method for solving the nonlinear difference equations which are generated by this discretization procedure can be derived by embedding the steady-state equation in an appropriate artificial time-dependent equation [8]. Thus the equations which are finally solved are a discrete approximation to the equation

$$\frac{\partial}{\partial X}(\rho h U + P)\ + \frac{\partial}{\partial Y}(\rho h V + Q)\ + \frac{\partial}{\partial Z}(\rho h W + R)$$

$$= \alpha\Phi_{XT} + \beta\Phi_{YT} + \gamma\Phi_{ZT} + \delta\Phi_T$$

where coefficients α, β and γ are chosen to make the flow direction timelike in zones of supersonic flow, as it is in the steady-state equation, and is a parameter related to the over-relaxation factor of a conventional relaxation process, which should be chosen to optimize the rate of damping [8, 14].

4 Application to swept wings

In the treatment of a particular geometric configuration the choice of the mesh will generally have an important influence on the accuracy which can be attained with a given number of mesh cells. The cells should be concentrated in regions where the disturbances in the flow are largest. Since the formulation of the artificial viscosity presupposes a smooth distribution of cells, and the one-point integration scheme will also cause a loss of accuracy if the mesh is irregular, it is important to use a reasonably smooth mesh. This is most easily accomplished by using global mappings to generate the mesh points.

The swept wing calculations presented in this section have been performed on meshes generated by the introduction of sheared parabolic coordinates [15]. First, parabolic coordinates are introduced in planes containing the wing sections by the transformation

$$\left(\bar{X} + i\bar{Y}\right)^2 = \frac{\{x - x_0(z) + i(y - y_0(z))\}}{t(z)}$$

$$\bar{Z} = z$$

where z is the spanwise coordinate, $t(z)$ is scaling factor which can be used to control the number of cells covering the wing, and $x_0(z)$ and $y_0(z)$ are the coordinates of a singular line just inside the leading edge which defines the origin of the parabolic coordinates. The effect of this transformation is unwrap the wing to form a shallow bump, $\bar{Y} = S(\bar{X}, \bar{Z})$, as illustrated in Fig.5.

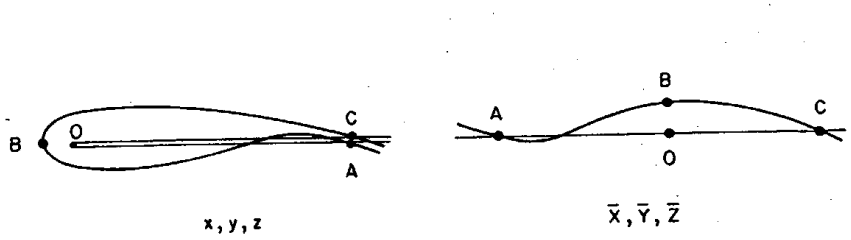

Fig. 5

Then a shearing transformation

$$X = \bar{X}, \quad Y = \bar{Y} - S(\bar{X}, \bar{Z}), \quad Z = \bar{Z}$$

is used to map the wing to the coordinate surface $Y = 0$. Finally the mesh points are constructed by the reverse sequence of mappings from a rectangular grid in the X, Y, Z coordinate system. The vortex sheet trailing behind the wing is assumed to coincide with the coordinate surface leaving the trailing edge. The definition of the mesh required by the finite-volume formulas consists simply of the cartesian co-ordinates of each mesh point, and a specification of which points lie on the boundary surfaces where special conditions are to be applied.

This mesh can be modified to treat wing-cylinder combinations by first mapping the cylinder to a vertical slit by a Joukowsky transformation, and then using the same sequence of transformations to generate a sheared parabolic coordinate system around the wing projecting from the slit. An alterative way of generating a mesh around a wing-fuselage combination [16] is to start by introducing cylindrical coordinates r and around the fuselage. In each cylindrical surface the wing section then appears as a profile in a channel bounded by the intersection of the surface with the plane of symmetry at $\theta = \pm\frac{\pi}{2}$. This configuration can be mapped to a channel with a bump on the upper wall by the transformation

$$\sigma = \log\left(1 - \cosh(\zeta)\right)$$

as illustrated in Fig.6. Finally the bump is removed by a shearing transformation.

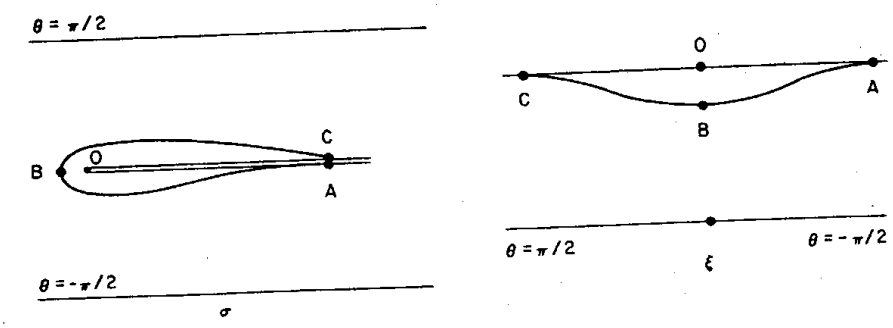

Fig. 6

Both these mesh-generating schemes lead to meshes which wrap around the leading edge of the wing, and belong to the second of three basic classes of mesh which are identified in Fig.7:

(a) Straight-through meshes in which one set of mesh lines is roughly parallel to the streamlines of the flow.

(b) Meshes wrapping around the leading edge of the wing and passing smoothly off the trailing edge.

(c) Meshes wrapping around both the leading and the trailing edge.

Consider a plane containing a wing section. Then meshes in class (a) can be generated by mapping the domain exterior to the profile onto the domain exterior to a slit, meshes in class (b) can be generated by mapping the domain exterior to the profile onto a half plane, and meshes in class (c) can be generated by mapping this domain onto the domain exterior to a disc. Depending on application, there may be advantages to any of these classes of mesh. Meshes in class (a) could be sheared to produce a mesh which is rectangular except in an inner region near the profile, and would lend themselves rather easily to a process of patching different meshes containing different components such as a wing and a tail.

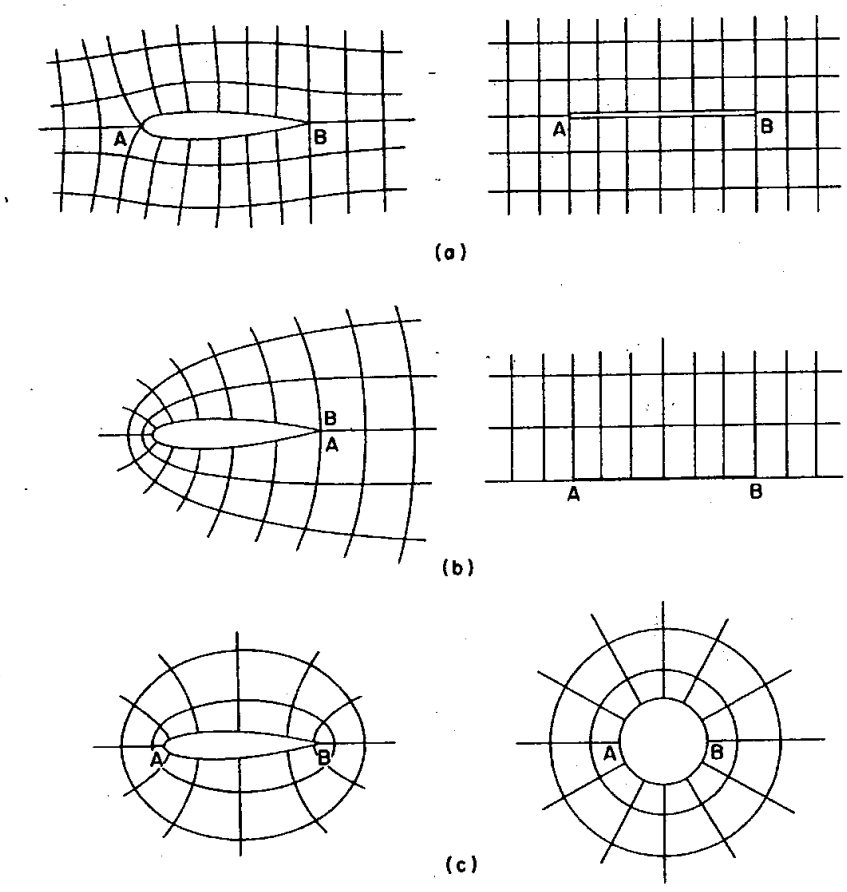

Fig. 7

On the other hand, they offer poor resolution in the region around the leading edge because of the singularity introduced by folding a smooth curve to a slit. Meshes in class (c) lead to a natural bunching of the cells near the trailing edge which leads to a good resolution of the Kutta condition, and have been demonstrated to give very accurate results in two-dimensional calculations [1,2]. The generation of meshes in class (c) requires the use of comparatively complicated mapping procedures, however, particularly in the framework of cylindrical coordinates, and the small mesh-width near the trailing edge can lead 'to a low rate of convergence of the iterative scheme.

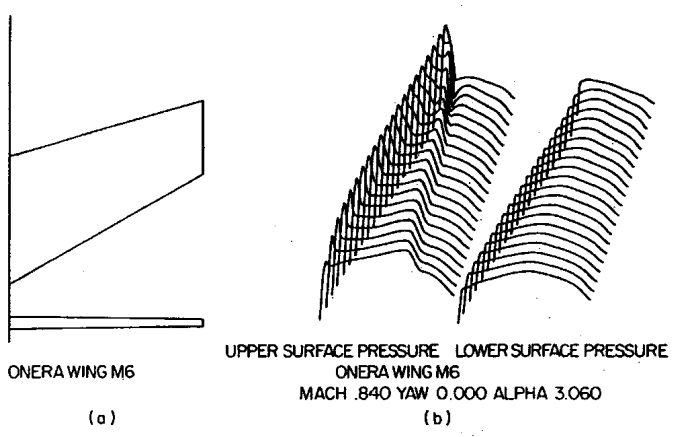

Fig. 8

Figs.8 and 9 show results of swept wing calculations. The first example is a calculation of the flow past the ONERA M6 wing, for which experimental data are available [17]. Separate pressure distributions are shown for stations at 20, 45, 65, and 95 percent of the semispan. Section lift and drag coefficients CL and CD were obtained by integrating the pressure coefficient at which the flow has sonic speed is marked by a horizontal line on the pressure axis. Although the calculation did not include any correction for the displacement effect of the viscous boundary layer, it can be seen that the agreement with the experimental data is quite good. The triangular shock pattern above the planform is clearly visible in the three-dimensional plot of the pressure distribution (Fig.8b). The front shock, emanating from the leading edge at the wing root, merges with the rear shock about three quarters of the way across the span. The mesh used in this calculation contained 160 intervals in the X direction wrapping around the section, 16 intervals in the Y direction normal to the section, and 32 intervals in the spanwise direction, for a total of 31, 820 cells. Preliminary calculations were performed on grids with 40x4x8 and 80x8x16 cells, and the result of each of these calculations was interpolated to provide the starting guess for the next mesh. 100 relaxation cycles were used on each mesh. Such a calculation takes about 15 minutes on a CDC 7600.

Fig.9 has been provided by the Boeing Company, and shows the result of a calculation which was performed at Boeing with the same code. The wing is a modern design with a quite highly cambered section and substantial rear loading. In this case a boundary layer correction was made, using a program developed by McLean to predict the displacement thickness of turbulent boundary layers in three-dimensional flow [18], and the correction has a significant effect.

The results of these calculations encourage confidence in the usefulness of the potential flow model for engineering predictions, and with the appearance of a new generation of computers one can reasonably contemplate the possibility of attempting a calculation for a complete aircraft, such as a Boeing 747.

References

[1] Bauer, F., Garabedian, P., Korn, D., and Jameson, A.: Supercritical Wing Sections II, Springer Verlag, New York, 1975.

[2] Jameson, Antony: Transonic flow calculations, in Numerical Methods in Fluid Dynamics, edited by M.J Wirz and J.J. Smolderen, Hemisphere, Washington, 1978.

[3] Ives, D.C., and Liutermoza, J.L.: Analysis of transonic cascade flow using conformal mapping and relaxation techniques, AIAA Journal, Vol. 15, 1977, pp. 647-652.

[4] Arlinger, B.G.: Calculation of transonic flow around axisymmetric inlets, AIAA Paper 75-80, 1975.

[5] Murman, E.M., and Cole, J.D.: Calculation of Plane steady transonic flows, AIAA Journal, Vol. 9, 1971, pp 114-121.

[6] Jameson, Antony: Numerical solution of nonlinear partial differential equations of mixed type, in Numerical Solution of Partial Differential Equations, III, SYNSPADE 1975, edited by B. Hubbard, Academic Press, New York, 1976.

[7] Lax, Peter, and Wendroff, Burton: Systems of conservation laws, Comm. Pure Appl. Math., Vol. 13, 1960, pp.217-237.

[8] Jameson, Anthony: Iterative solution of transonic flows over airfoils and wings, including flows at Mach 1, Comm. Pure Appl. Math., Vol. 27, 1974, pp. 283-309.

[9] Glowinski, R., Periaux, J., and Pironneau, O.: Transonic flow simulation by the finite element method via optimal control, Proceedings of the Second International Symposium in Flow Problems, Santa Margherita, June 1976.

[10] Morawetz, C.S.: On the nonexistence of continous transonic flows past profiles, Comm. Pure Appl. Math., Vol. 9, 1956, pp. 45-68.

[11] Bateman, H.: Notes on a differential equation which occurs in the two-dimensional motion of a compressible fluid and the associated variational problem, Proc. Roy. Soc. Series A, Vol. 125, 1929, pp. 598-618.

[12] Synge, J.L., and Schild, A.: Tensor Calculus, University of Toronto Press, 1949, pp. 57-58.

[13] Strang, G., and Fix, G.J.: An analysis of the Finite Element Method, Prentice Hall, Englewood Cliffs, N.J., 1973.

[14] Garabedian, P.R.: Estimation of the relaxation factor for small mesh size, Math. Tables Aids Comp., Vol. 10, 1956, pp. 183-185.

[15] Jameson, Antony, and Caughey, D.A.: A finite volume method for transonic potential flow calculations, Proceedings of Third AIAA Conference on Computational Fluid Dynamics, Albuquerque, June 1977.

[16] Caughey, D.A., and Jameson, Antony: Numerical calculation of transonic potential flow about wing fuselage combinations, AIAA Paper 77-677, 1977.

[17] Monnerie, B., and Charpin, F.: Essais de buffeting d'une aile an fleche en fleche en transsonique, 10e Colloque d'Aerodynamique Appliquee, Lille, November 1973.

[18] McLean, J.D.: Three-dimensional turbulent boundary layer calculations for swept wings, AIAA Paper 77-3, 1977.

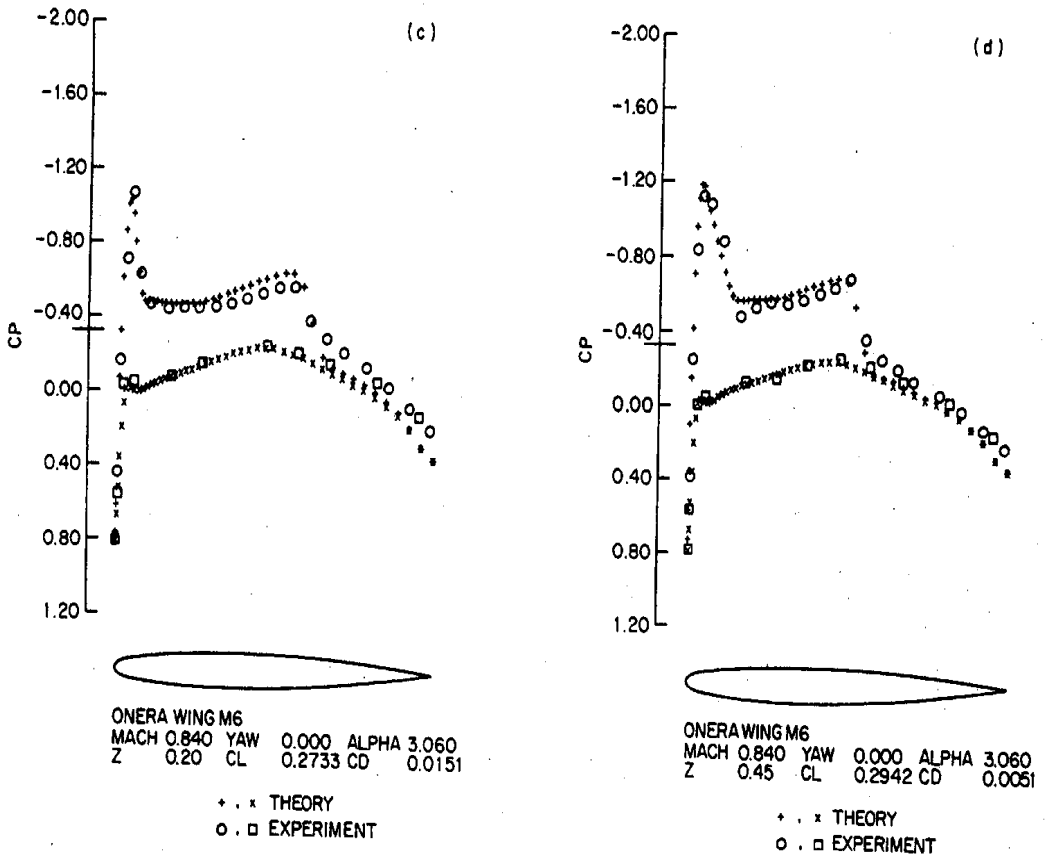
(c)
-2.00
-1.60
-1.20
-0.80
-0.40
0.00
0.40
0.80
1.20
CP
ONERA WING M6
MACH 0.840 YAW 0.000 ALPHA 3.060
Z 0.20 CL 0.2733 CD 0.0151
+ . x THEORY
o . □ EXPERIMENT
(d)
-2.00
-1.60
-1.20
-0.80
-0.40
0.00
0.40
0.80
1.20
CP
ONERA WING M6
MACH 0.840 YAW 0.000 ALPHA 3.060
Z 0.45 CL 0.2942 CD 0.0051
+ . x THEORY
o . □ EXPERIMENT

Fig. 8

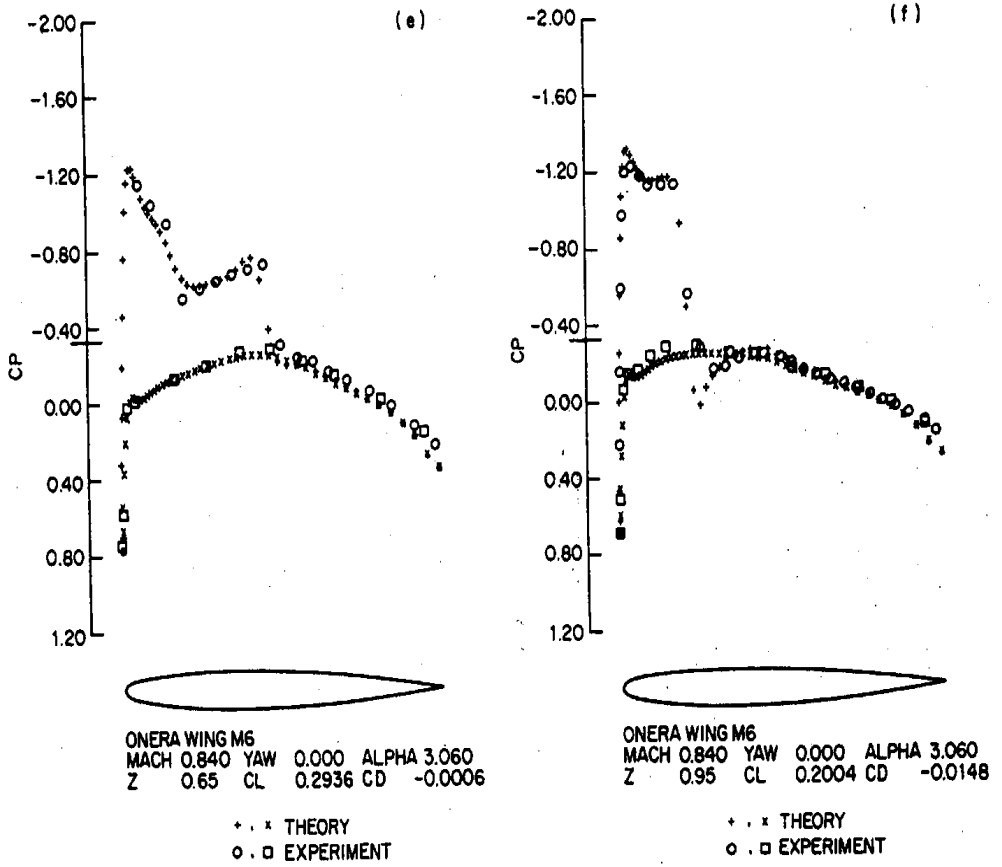
(e)
-2.00
-1.60
-1.20
-0.80
-0.40
CP
0.00
0.40
0.80
1.20
ONERA WING M6
MACH 0.840 YAW 0.000 ALPHA 3.060
Z 0.65 CL 0.2936 CD -0.0006
+ . x THEORY
o . □ EXPERIMENT
(f)
-2.00
-1.60
-1.20
-0.80
-0.40
CP
0.00
0.40
0.80
1.20
ONERA WING M6
MACH 0.840 YAW 0.000 ALPHA 3.060
Z 0.95 CL 0.2004 CD -0.0148
+ . x THEORY
o . □ EXPERIMENT

Fig. 8

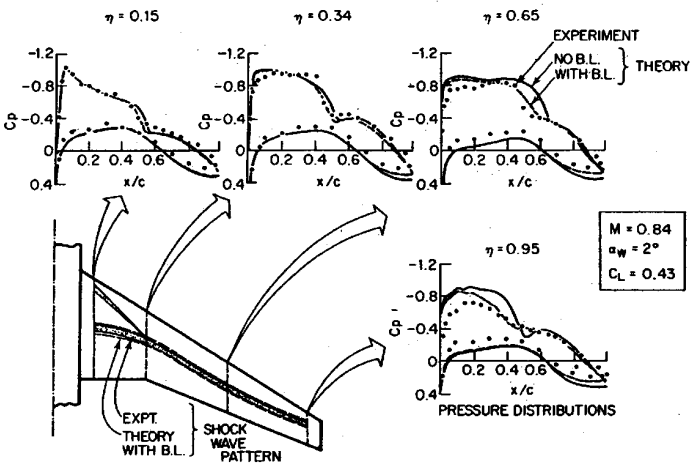
η = 0.15
η = 0.34
η = 0.65
EXPERIMENT
NO B.L.
WITH B.L.
THEORY
-1.2
-0.8
-0.4
0
0.4
Cp
0.2 0.4 0.6
x/c
M = 0.84
αW = 2°
CL = 0.43
η = 0.95
PRESSURE DISTRIBUTIONS
EXPT.
THEORY
WITH B.L.
SHOCK
WAVE
PATTERN

Fig. 9